ГИАБ. Горный информационно-аналитический бюллетень /
MIAB. Mining Informational and Analytical Bulletin, 2020;(7):27-44
ОРИГИНАЛЬНАЯ СТАТЬЯ / ORIGINAL PAPER

УДК 552.541:552.08 DOI: 10.25018/0236-1493-2020-7-0-27-44

ВЛИЯНИЕ СВЯЗНЫХ ГРАНИЦ РАЗДЕЛА ДОЛОМИТ-ГИПС НА АКУСТИЧЕСКИЕ СВОЙСТВА И ПОВРЕЖДЕННОСТЬ ГОРНОЙ ПОРОДЫ ПРИ ЦИКЛИЧЕСКИХ ИЗГИБНЫХ НАГРУЖЕНИЯХ

А.С. Вознесенский[1], М.Н. Красилов[1], Я.О. Куткин[1], А.О. Тютчева[1]

[1] ГИ НИТУ «МИСиС», Москва, Россия, e-mail: al48@mail.ru

Аннотация: Рассмотрено изменение скоростей упругих волн C_p, C_{s1}, C_{s2} и акустической добротности Q балок породы при циклическом изгибе. Образцы содержали связные границы доломит-гипс сложной текстуры. Измерялись количество циклов нагружения и параметр поврежденности ω. Эксперименты проводились на образцах-балках пород Новомосковского месторождения гипса (Тульская область, Россия) при изгибе по трехточечной схеме. В верхней части образца находился, в основном, слой доломита, который обладал более высокой прочностью, меньшими акустическими потерями и более высокой акустической добротностью по сравнению с гипсом, расположенным преимущественно в нижней части образца. Переход между доломитом и гипсом имел сложную пятнистую текстуру с чередованием обоих минералов. Эксперимент проводился сериями по 100 циклов загрузки / разгрузки. Скорости продольных и поперечных (вдоль и поперек направления нагрузки) упругих волн, а также акустическая добротность измерялись до испытания и между циклами. Максимальная нагрузка цикла в каждой последующей серии увеличивалась по сравнению с предыдущей серией, чтобы найти режим малоцикловой усталости. Скорости упругих волн уменьшались, а акустическая добротность возрастала при увеличении количества усталостных циклов. Непосредственно перед разрушением добротность Q показала резкое снижение, связанное с разрушением матрицы. Моделирование методом конечных элементов подтвердило гипотезу, что увеличение добротности связано с ослаблением прочности контактов на границах между высокодобротным доломитом и низкодобротным гипсом. Параметр поврежденности ω оценивался как отношение общего количества событий АЕ с начала эксперимента к общему количеству событий АЕ при разрушении. Определена точность регрессионных зависимостей оценки параметра поврежденности ω по акустическим свойствам при их различном количестве.

Ключевые слова: горные породы, связная граница, доломит-гипс, сложная текстура, акустический, упругие волны, скорость, добротность.

Благодарность: Работа выполнена при финансовой поддержке Российского фонда фундаментальных исследований (РФФИ), Россия, грант № 20-05-00341.

Для цитирования: *Вознесенский А. С., Красилов М. Н., Куткин Я. О., Тютчева А. О.* Влияние связных границ раздела доломит-гипс на акустические свойства и поврежденность горной породы при циклических изгибных нагружениях // Горный информационно-аналитический бюллетень. – 2020. – № 7. – С. 27–44. DOI: 10.25018/0236-1493-2020-7-0-27-44.

The effects of dolomite-gypsum bonded interfaces on acoustic properties and damage of rock under cyclic bending loads

A.S. Voznesenskii[1], M.N. Krasilov[1], Ya.O. Kutkin[1], A.O. Tyutcheva[1]

[1] Mining Institute, National University of Science and Technology «MISiS», Moscow, Russia, e-mail: al48@mail.ru

Abstract: The change in the elastic wave velocities C_p, C_{s1}, C_{s2} and the acoustic quality factor Q of rock beams under cyclic bending loading are considered in the article. The specimen contained bonded dolomite-gypsum boundaries of complex structure. The number of loading cycles and damage parameter ω were registered.The experiments were carried out on rock specimens from the Novomoskovsk gypsum field (Tula region, Russia) with bending by a three-point scheme. The upper part of the sample was mainly a layer of dolomite, which had higher strength, lower acoustic loss and higher acoustic quality factor compared to gypsum (which was located mainly in the lower part of the sample). The interface between dolomite and gypsum had a complex spotty texture with the alternation of both minerals. The experiment was carried out in a series of 100 load/unload cycles. The velocities of the longitudinal and transverse elastic waves (along and across the direction of loading), as well as the acoustic Q factor, were measured before and between cycles. The maximum load of the cycle in each subsequent series was increased in comparison with the previous series to find the mode of low cycle fatigue. The elastic wave velocities decreased and the acoustic Q factor increased with an increase in the number of fatigue cycles. Just before destruction, the Q factor showed a sharp decrease associated with the destruction of the matrix. Modeling by the finite element method confirmed the hypothesis that an increase in the quality factor is associated with a weakening of contacts at the boundaries between high-quality dolomite and low-quality gypsum. The damage parameter ω was estimated as the ratio of the total number of AE event count from the beginning of the experiment to the total number of AE event count at destruction. The accuracy of the regression dependencies of the damage parameter ω by the acoustic properties is determined for various amounts.

Key words: rock, bonded boundary, dolomite-gypsum, complex structure, acoustic, elastic waves, velocity, quality factor.

Acknowledgements: This work was carried out under the auspices of the Russian Foundation for Basic Research (RFBR) – Russia, Grant No. 20-05-00341.

For citation: Voznesenskii A.S., Krasilov M.N., Kutkin Ya.O., Tyutcheva A.O. The effects of dolomite-gypsum bonded interfaces on acoustic properties and damage of rock under cyclic bending loads. *MIAB. Mining Inf. Anal. Bull.* 2020;(7):27-44. [In Russ]. DOI: 10.25018/0236-1493-2020-7-0-27-44.

Introduction

State of the art

Bonded and un-bonded boundaries between rocks of various types have a significant impact on the strength properties of rocks and massifs. It has been noted in a number of studies, that knowledge of the mechanical properties of these boundaries is necessary for predicting rock bursts and coal bumps [1], failure slopes of quarries and slides [2], roof fall in underground workings [3], the hydraulic fracturing of rocks [4], the design of concrete lining in tunnels [5] and piles to strengthen slopes [6], ensuring the tightness of underground storage of gas, oil, radioactive and chemical wastes [7] and to solve other geotechnical problems.

It should be noted that many objects in rock massifs, and the boundaries between the rocks, are affected by the cyclic loads arising from blasting operations [8, 9], injections and selection of fluids in underground storage facilities [10], reservoirs during production intensification of heavy and superheavy oil [11], in areas of increased seismicity [12], and when traffic is moving along the workings at great depths [13]. This determines the need to study the cyclic effects on the strength properties of rocks, in general, and the boundaries contained in them, between rocks of various types.

Among the strength properties and the factors influencing them, the ultimate tensile strength, damage [14], defects [15] and cracks [16] are considered.

The tensile strength characterises the maximum allowable stresses and, for intermediate estimates, the damage parameter ω [17], introduced by Yu.N. Rabotnov, and the integrity parameter ψ [18], introduced by L.M. Kachanov, allow us to evaluate strength in the range between its limits and complete absence.

It is not always possible to monitor parameters ω and ψ continuously, for example, using the acoustic emission method (AE) [19, 20]. It is advisable to use other acoustic methods [21] in these cases. The most widely used informative acoustic parameters include the velocities of longitudinal and transverse elastic waves, as well as the less frequently used acoustic *Q* quality factor. This makes it possible to estimate the damage parameter ω from regression dependences, by periodic single measurements of acoustic properties.

The purpose and objectives of the study

The main goal of this study was to assess the effect of the bonded boundaries between gypsum and dolomite on the changes in acoustic properties at various degrees of damage, as well as on the relationship of the damage parameter ω with elastic wave velocities and acoustic quality factor *Q*. The tasks included the development of a method for changing the damage of samples due to fatigue and cyclic bending loads of specimen-beams with a quantitative assessment of the damage parameter from the total AE, as well as justification of the model of physical mechanisms for changing the acoustic quality factor in such tests. Another task was the construction of regression dependencies between parameter ω and the velocities of elastic waves and acoustic quality factor, with an assessment of the accuracy of such dependencies.

Materials and methods

Rock samples

The experiments were carried out on beam specimens of gypsum-containing rocks from the Novomoskovsk field in the Tula region of Russia, while bending in the three-point scheme. The deposit is mined underground by a drilling and blasting method. The samples had the form of beams with dimensions of 40× 40×200 mm. 12 samples were tested in total. Of these, five samples were tested to determine the tensile strength by bending tests. The testing procedure and measurements were worked out on four samples. The main results were obtained on three samples G-2-04-AE, G-2-18-AE and G-2-05-AE. The samples had a complex, two-phase layered structure and included areas of spotted gypsum and dolomite. The photograph in Fig. 1(a) shows an example of their structure on one side of sample G-2-5-AE. Fig. 1(b) depicts the approximate location of the minerals. The dolomite areas are light and the gypsum areas are shaded, in this diagram. The letter T shows the position of the electric strain gauge in the lower part of the beam for detecting tensile deformations under cyclic loading. Black triangles mark the points of applica-

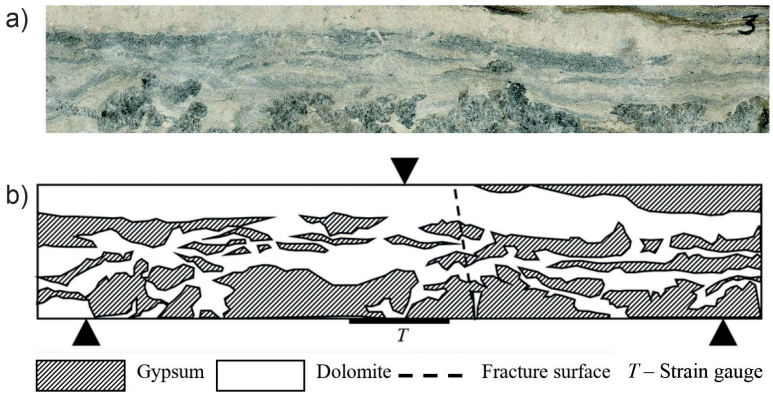

Fig. 1. Side view of a beam specimen of rock with the boundaries of dolomite-gypsum (a) and the approximate location of minerals (b)

Рис. 1. Вид сбоку на образец-балку гипсосодержащей породы (а) и ориентировочное расположение минералов (б)

tion of the bending loads. The dashed line indicates the position of the fault plane after the specimen was destroyed.

In the upper part of the sample, there was a layer of dolomite which had higher strength, lower acoustic losses and a higher acoustic quality factor compared to gypsum, which was mainly seen in the lower part of the sample. The border interface between dolomite and gypsum had a complex spotty structure due to the alternation of both minerals. This feature manifested itself in the resulting acoustic and deformation dependencies, as analysed below.

Testing: main ideas, methodology and sequence of operations

The complex method of investigation included mechanical and acoustic measurements of various informative parameters in the process of cyclic loading of the rock samples.

Cyclic mechanical fatigue loadings were carried out in a series of 100 cycles, to create certain damage in rock samples. The minimum load in the cycle was 3 to 5% of the average ultimate bending strength (UBS). The maximum load in the cycle series did not change and it increased in the subsequent series compared to the previous one. The initial UBS was determined as being the average value from the destruction of five samples. As shown by preliminary testing, the deformation and fatigue could be divided into several modes, depending on the maximum load in the cycle.

The elastic deformation mode (the first mode) manifests itself in high cycle fatigue. The plastic deformation mode manifests itself in low cycle fatigue (the second mode). The brittle fracture mode (the third mode) manifests itself by instantly destroying the specimen. The load of the third mode is greater than the load of the second mode, which is greater than the load of the first mode. An increase in the load in each subsequent series with AE monitoring was chosen to ensure low-cycle fatigue. This solution made it possible to determine the transition to the low cycle fatigue mode up to the destruction of the sample and to carry out tests within the allowable time.

The velocities of the longitudinal (C_p) and transverse (C_{s1} and C_{s2}) elastic waves (with polarisation planes in and across the load direction, accordingly), as well as the acoustic quality factor Q of the samples, were measured before commencement of each test, and between the loading series.

Acoustic quality factor Q physically characterises the ratio of the total energy of a system to its losses in one oscillation period. It was determined by resonant acoustic spectroscopy [22] during rock sample excitations with the harmonic signal of the elastic waves and were calculated according to:

$$Q = \frac{f_0}{f_{\max} - f_{\min}}, \qquad (1)$$

where f_0 is the resonant frequency. This frequency is determined by the maximum amplitude of harmonic signal of the sample at the measurement. $f_{\max}$ and $f_{\min}$ are the upper and lower band frequencies of the signal at the $1/\sqrt{2}$ level of the maximum amplitude value at the resonance.

To assess the destruction of the sample, the authors chose the damage parameter ω, which varies from 0 to 1 and is generalised. This parameter characterises a decrease in the effective value of the cross-sectional area of the structural element under consideration. It can evaluate the change in strength of a particular sample or material in accordance with the ratio

$$\sigma_s(\omega) = \sigma_{s0}(1 - \omega), \qquad (2)$$

where $\sigma_s(\omega)$ and σ_{s0} are the current and initial strength values, accordingly.

This makes it possible to estimate the strength of one sample without effecting the dispersion of the sample group properties.

The tests were carried out in the following sequence:

1. Measurements of the elastic wave velocities and acoustic Q factor were made. The elastic wave velocities were measured by elastic impulse propagation time. The acoustic quality factor was measured by the resonance method.

2. The maximum load of the first series was set. The sample was loaded in a series of 100 cycles. The load and vertical displacements of the beam in the middle part, as well as the readings of the strain gauge glued to the bottom of the sample, and the AE event count rate were recorded.

3. If the sample in the series was not destroyed, the elastic wave velocities and Q factor were measured again, in accord-

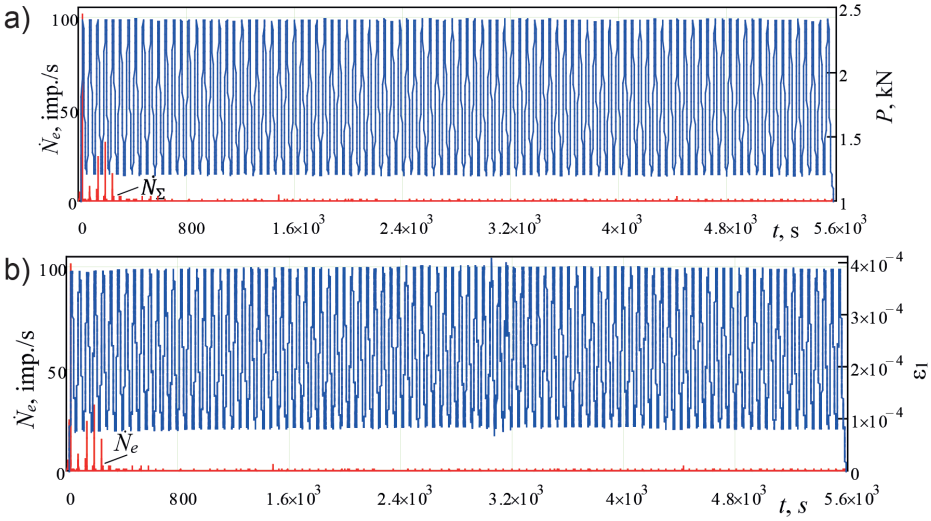

Fig. 2. Graphs of dependencies on time for the specimen load P (a) and gauge strain ε_1 (b), as well as AE event count rate $\dot{N}_e$ under cyclic bending loads, with a maximum load of 2,40 kN

Рис. 2. Графики зависимостей от времени для нагрузки образца P (a) и калибровочной деформации ε_1 (b), а также скорости счета событий AE $\dot{N}_e$ при циклических изгибающих нагрузках с максимальной нагрузкой 2,40 кН

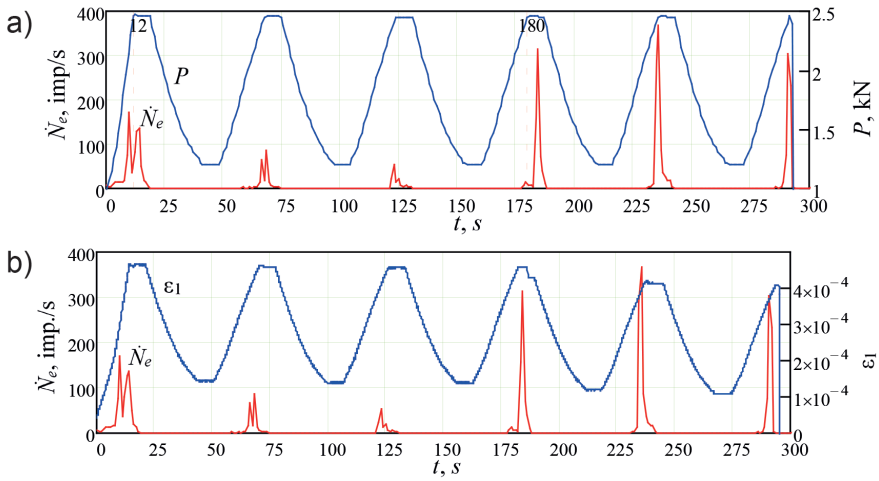

Fig. 3. Graphs of dependencies on time of the specimen load P (a) and relative deformations of the strain gauge ε_1 (b) and the event count rate $\dot{N}_e$ under cyclic bending loads, with a maximum load of 2,45 kN

Рис. 3. Графики зависимостей от времени нагрузки образца P (a) и относительных деформаций тензодатчика ε_1 (b) и активности АЭ $\dot{N}_e$ при циклических изгибающих нагрузках с максимальной нагрузкой 2,45 кН

ance with clause 1. Then, the maximum load in the cycle was increased and the tests were carried out at the next series, as described in the previous paragraph.

4. If the sample was destroyed, the test was terminated.

Testing and measurement equipment

The laboratory setup consists of mechanical and acoustic parts. Mechanical tests were carried out with an «ASIS» automated testing system, made by NPO Geotech Ltd (Russia). The loading and deformation of the rock samples was carried out using a computer-controlled stepping motor. A more detailed description of the base part was given in [23]. The three-point loading scheme complied with the testing of rock samples during bending.

The acoustic testing subsystem developed by EcogeosProm LLC (Tver, Russia), provided measurements of the velocities of longitudinal and transverse elastic waves. The acoustic quality factor was also measured by a resonance method using a setup developed by the authors. In addition,

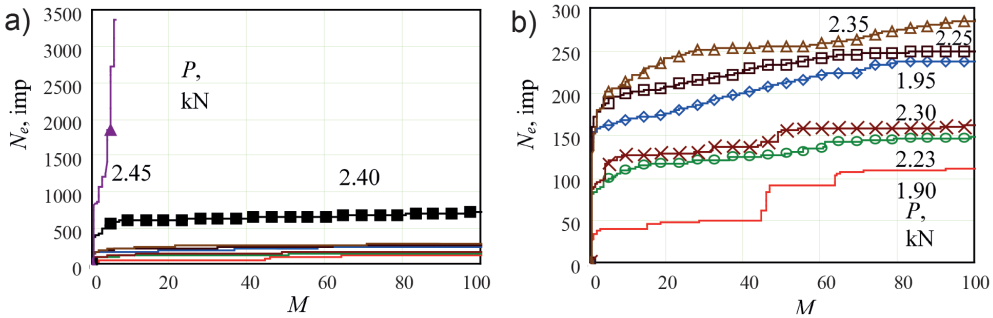

Fig. 4. Graphs of AE event count N_e dependencies versus number of cycles M at various loads at different scales of the vertical axis (a) and (b)

Рис. 4. Графики зависимости числа событий АЭ N_e от количества циклов M при различных нагрузках в разных масштабах вертикальной оси (a) и (б)

a QM-Box system with an AF-15 device (R-Technology LLC, Moscow, Russia) recorded AE pulses in the frequency range from 20 to 200 kHz during a series of fatigue loading. This subsystem recorded the full waveform and the AE event count rate $\dot{N}_e$, which were displayed on the computer screen during the experiments. It allowed their progress to be monitored.

Results

Mechanical observations

The test results from the G25AE sample at maximum load *P* in a cycle equal to 1,9 kN versus time *t* are shown below, in the form of graphs in Figs. 2(a) and (b).

Each loading series consists of 100 loading-unloading cycles, as marked in Fig. 2(a). The same graph shows the dependence of the AE event count rate $\dot{N}_e$, the maximum value of which is 103 imp./s, and then decreases with each cycle to 1–2 imp./s. Fig. 2(b) shows the corresponding changes in the tensile strain gauge. The upper part of Fig. 2(b) corresponds to tension and the lower part to compression of the strain gauge. In this form, they repeat the graph of the load change, which indicates a significant degree of the sample deformation in the elastic region.

Figs. 3(a) and (b) show the load chang. P and the readings of the strain gauge at 2,45 kN. Here, the sample collapsed during the 6th cycle, in contrast to the previous series.

In Fig. 3(a), the load increases and stabilises up to 12 s. In this graph, $\dot{N}_e$ shows the increase before this moment, and then the decrease. There is a subsequent increase and decrease, which is associated with the stabilisation of the load carried out by the press control system. The amplitude in the first part is larger than the second part. A similar increase in $\dot{N}_e$ on the 4th cycle at 180 s shows the inverse relationship. The value $\dot{N}_e$ in the first part is less than that in the second part. This indicates the approach of the destruction of the sample. For the same series, the strain gauge is compressed, which indicates a decrease in tensile strain due to crack growth, as shown in Fig. 1(b).

AE observations

The results of the AE event count N_Σ registration versus the number of cycles *M* for the entire observation period on an overview scale and are presented in Fig. 4(a). In addition, the curves obtained for loads from 1,90 to 2,35 kN are also shown in Fig. 4(b), for a distinct image on an extended scale.

The graphs in Fig. 4(a) show a slight increase in the AE event count on the steps with loads from 1,90 to 2,35 kN, compared with the load of 2,40 kN and, in particular, 2, 5 kN. The graphs in Fig. 4(b) show that, in the first series, the discrete nature of the AE is observed, which is expressed in a stepped, spasmodic course of curves. The nature of the curve changes at a load of 2,35 kN demonstrate a smoother change. It should also be noted that the curves have a smooth course with a large number of cycles.

Changes in acoustic properties

Fig. 5 presents the measurements of acoustic properties, depending on the test series. The velocity of the longitudinal waves C_p in Fig. 5(a) initially increases, with increasing load, and then decreases. It does not show significant changes at *M* = 400 and above. The velocities of the transverse waves C_{s1} and C_{s2} in Fig. 5(b) initially decrease but they do not show significant changes at *M* = 400 and above, similar to C_p.

The graphs showing the *Q* factor change are presented in Figs. 5(a) and (b) for comparison with the velocity graphs. The *Q* factor shows an increase up to *M* = 600 and then decreases until speci-

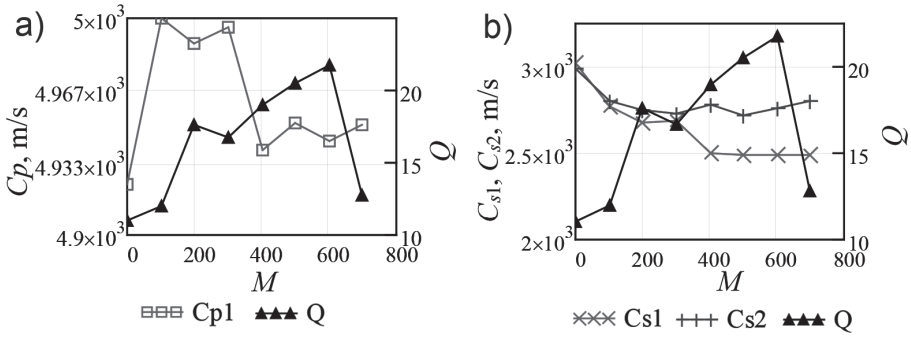

Fig. 5. Changes in velocity of the longitudinal waves Cp and the acoustic quality factor Q (a), as well as the velocities of the transverse waves C_{s1} and C_{s2} and the quality factor Q (b) depending on the number of load cycles M

Рис. 5. Изменения скорости продольных волн Cp и добротности Q (a), а также скоростей поперечных волн C_{s1} и C_{s2} и добротности Q (b) в зависимости от количества циклов нагрузки M

men failure. Measurements of the acoustic properties at M = 600 characterise the specimen state before its destruction, since it occurred on the 6th loading cycle in the next series.

Discussion

Mechanical precursors of destruction

The comparison of load and strain measurement graphs for the strain gauge at 2,40 kN (presented in Figs. 2(a) and (b)) with graphs at lower loads, showed their complete identity. Therefore, purely mechanical measurements cannot predict the destruction of the samples.

The initial part of the curves up to three cycles (presented in Figs. 3(a) and (b)) shows that the load and strain graphs at 2,45 kN do not qualitatively differ from the graphs obtained on the steps with a lower maximum load in the cycles. Simultaneously, an abrupt decrease in the resistance of the strain gauge was observed in the 4th cycle. This corresponds with a reduction in the tensile strain and indicates the germination of a macro crack during the sample destruction, with its exit outside the strain gauge in the 6th cycle when the sample was destroyed. Fig. 1 shows the scheme of the crack with a dotted line.

The conclusion can be drawn that, during fatigue cyclic bending loads, the mechanical observations cannot reveal the proximity of fractures in the early stages of the destruction of the sample material but can provide information regarding this immediately before fracture, when this process is already actively developing.

AE analysis and evaluation of damage parameter

The registration of AE allowed us to specify the load at which fatigue low cycle failure occurred. In this case, the load was 2,45 MPa. The decrease in the AE event count rate $\dot{N}_e$ occurred in the first three cycles in this series. It increased in the next three cycles immediately before destruction, as shown in Figs. 3(a) and (b).

In addition, it provided an opportunity to assess the damage parameter after each series of loads. For this, the total number of the event count after each i-th series $\Sigma N_{\Sigma i}$ and this one after specimen destruction N_f were calculated. In this case, N_f = = 5226 imp. The calculated results are shown in Table 1.

In Table 1, N_{ei} is the AE event count at the i-th series and ΣN_{ei} is the sum of the AE event count from the beginning of the experiment to the end of the i-th series.

The damage assessment was carried out using the damage parameter ω introduced by Rabotnov. This parameter characterises the reduction of the effective cross-sectional area of the sample. The value ω = 0 characterises the undisturbed material and ω = 1 when destroyed. In our case, the damage parameter was estimated using [24]:

$$\omega_i = \frac{\Sigma N_{ei}}{N_f}, \quad (3)$$

where ω_i is the current value of the damage parameter after each *i*-th series of loads, ΣN_{ei} is the current value of the total AE event count from the beginning of the experiment and N_f is the total AE event count at destruction, N_f = 5226 imp. The damage values after each series of cyclic loads on specimen G-2-5-AE are graphically shown in Fig. 6. The graphs were made in 100 cycle increments, corresponding to each series. The dependence obtained is used below and represents the relationship between acoustic and damage parameters.

The obtained dependencies between the number of loading cycles *M* and the damage parameter ω allowed us to further calculate and plot the dependencies of the damage parameter on the acoustic properties.

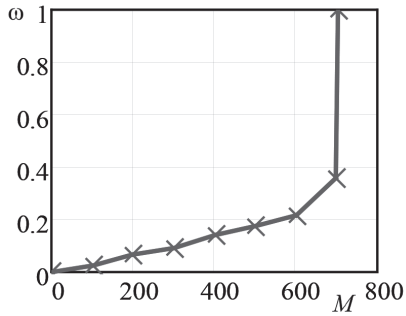

Fig. 6. Change in damage parameter ω versus number of cycles M when testing sample G-2-5-AE
Рис. 6. Изменение параметра поврежденности ω в зависимости от количества циклов M при испытании образца G-2-5-AE

Relationships between damage and acoustic properties

Table 2 presents data for the damage parameter, maximum load in cycles and acoustic properties depending on the number of fatigue loading cycles *M* from the beginning of the experiment. These data, in units relative to the average value depending on the damage, are given for clarity in the graphs below.

The last row of Table 2 contains empty cells, since it corresponds to destruction, when the acoustic parameters were not measured.

Table 1

Maximum number of event count at each series of cyclic loading and the forecast of the damage parameter
Максимальное количество событий в каждой серии циклических нагрузок и прогноз параметра поврежденности

Series number, *i*	P_{maxi}, kN	AE event count N_e	Sum of AE event count ΣN_{ei}	Damage parameter ω
0	0,00	0,00	0	0,00
1	1,90	110	110	0,021
2	1,95	238	348	0,067
3	2,23	150	498	0,095
4	2,25	249	747	0,143
5	2,30	164	911	0,174
6	2,35	238	1149	0,220
7	2,40	711	1860	0,356
8	2,45	3366	Nf = 5226	1,000

Table 2

Damage parameter and acoustic properties versus number of cycles
Параметр поврежденности и акустические свойства в зависимости от количества циклов

M	ω	*P*, kN	C_{p1}, m/s	C_{s1}, m/s	C_{s2}, m/s	*Q*	Q_d, 1/cycle
0	0,000	0,00	4923	3022	2991	11,0	0,000
100	0,021	1,90	5000	2773	2800	12,0	0,010
200	0,067	1,95	4988	2674	2750	17,6	0,056
300	0,095	2,23	4996	2685	2726	16,7	–0,009
400	0,143	2,25	4939	2500	2786	19,0	0,023
500	0,174	2,30	4952	2491	2718	20,5	0,015
600	0,220	2,35	4943	2490	2762	21,8	0,013
700	0,356	2,40	4951	2487	2800	12,8	–0,090
706	1,000	2,45	–	–	–	–	–

Fig. 7(a) shows the graphs of the relative velocity of the longitudinal waves C_p and the acoustic quality factor *Q* as a ratio to their first values C_{p0} and Q_0, and as a function of the damage parameter ω. An increase in both C_p and *Q* with increasing ω attracts attention. This can be explained by the structure of the sample; the upper part contains a more durable layer of dolomite. It has a higher velocity and elastic modulus, less attenuation of elastic waves and a higher quality factor *Q* compared to gypsum, which is located mainly in the lower part of the beam. Simultaneously, an increase in sample fracture primarily leads to the separation of gypsum lenses from the dolomite layer at the borders and to the preferential propagation of elastic waves through the dolomite. The overall result is an increase in both velocities and quality factor.

The described mechanism was modelled by numerical methods, which confirmed its reliability. Fig. 7(a) shows the graph of the modelled acoustic quality factor Q_{mod}, which increases as ω grows. A similar change in *Q* and Q_{mod} confirms the hypothesis of a physical mechanism

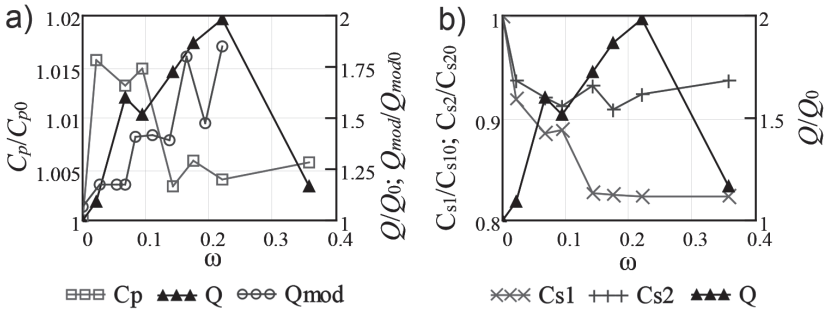

Fig. 7. Dependencies of the relative values of the longitudinal waves velocity C_p, the measured Q and modelled Q_{mod} of the acoustic Q factor (a), as well as the relative velocities of the transverse waves C_{s1} and C_{s2} (b) on the damage parameter ω

Рис. 7. Зависимость относительных значений скорости продольных волн C_p, измеренной Q и модельной Q_{mod} акустической добротности (a), а также относительных скоростей поперечных волн C_{s1} и C_{s2} (b) от параметра поврежденности ω

for the increase in acoustic quality factor with increasing ω. A description of the model is presented below.

Failure at the borders between gypsum and dolomite occurs with a further increase in damage and also their destruction, which causes a decrease in Q immediately before destruction at $\omega = 0{,}356$. It should be noted that the velocity of longitudinal waves only varies considerably in the early stages of damage accumulation. It shows no noticeable change immediately before destruction. The relative changes in C_p are small and do not exceed 2% of the first value, i.e. they are comparable with measurement errors of this kind, which indicates a low informative value of this parameter.

Simultaneously, the relative changes in Q are significantly larger than that of C_p. A sharp decrease in the quality factor between $\omega = 0{,}220$ and $\omega = 0{,}356$ is a sign of the approach of destruction.

Fig. 7(b) shows similar dependencies of the velocities of transverse elastic waves C_{s1} and C_{s2}, measured in the direction of polarisation along and across the direction of loading of the sample, respectively. These informative parameters exhibit high sensitivity at low values of damage and weakly reflect the effect of damage at $\omega > 0{,}14$, as well as for the velocity of longitudinal waves C_p. The relative changes in the velocities of the transverse waves are within 20%, which is greater than that of the longitudinal wave but smaller than that of Q.

It should be noted that similar dependencies of an increase in the Q factor with an increase in damage, followed by a decrease of Q before the series at which the destruction occurred, were noted for all three samples. The indicated dependencies in the region of increasing Q of the samples are approximated by linear functions:

$\delta Q = 2{,}74P - 1{,}39$; $R = 0{,}64$ for G-2-04-AE,

$\delta Q = 5{,}03P - 4{,}40$; $R = 0{,}95$ for G-2-18-AE,

$\delta Q = 3{,}68P - 2{,}63$; $R = 0{,}93$ for G-2-05-AE,

where $\delta Q = Q(P)/Q_0$ is the relative Q factor, $\delta P = P/P_0$ is the relative maximum load, Q_0, P_0 are the first values of the Q factor and maximum load in a series of tests, respectively.

The variation in the values of the coefficient of proportionality at P is mainly due to the difference in the properties of the samples, as well as to a lesser extent, the first value of the maximum load to which the tests began. That is, all three samples showed the presence of a plot of increase in acoustic quality factor, which gives rise to the assumption of the same mechanism of this phenomenon.

Modelling of changes in acoustic Q-factor depending on the boundary damage between dolomite and gypsum

A numerical model was developed in the COMSOL Multiphysics environment to test the hypothesis about the effect of the destruction of the boundaries between dolomite and gypsum on the increase in acoustic quality factor.

Fig. 8(a) presents the drawing of the model and Fig. 8(b) presents its grid diagram. Piezoelectric transducers are located above and below, on the top of which a linear frequency-modulated (LFM) model electric signal was supplied, and a signal characterising the resonance properties of the sample was taken from the bottom. The mechanical properties of the rocks were taken from preliminary experiments.

Regression dependencies for calculating the damage parameter by acoustic properties and accuracy estimation

In general, the following can be noted from the point of view of the reliable assessment of damage and the prediction of fractures under bending loads of rock containing gypsum-dolomite borders. The acoustic quality factor has maximum in-

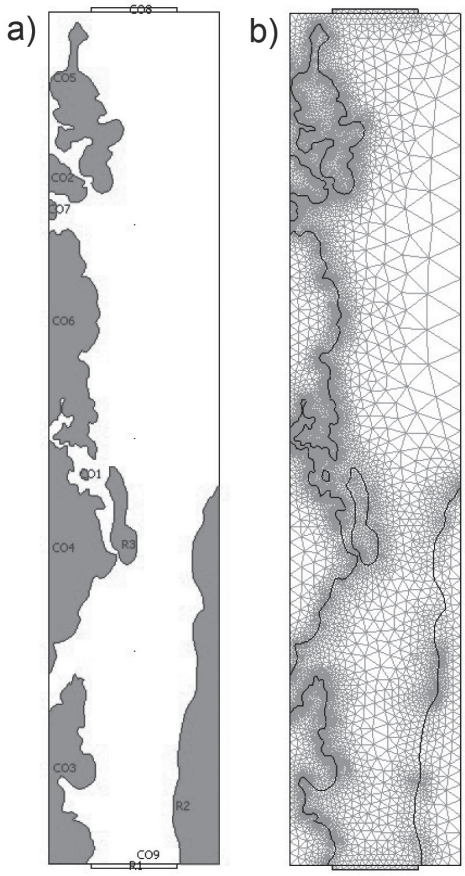

Fig. 8. Drawing of the model (a) and its grid diagram (b); light areas in (a) indicate dolomite; dark areas indicate gypsum

Рис. 8. Чертеж модели (а) и ее разбивка по сетке (b); светлые области – доломит, темные – гипс

formation content and then the shear wave velocities follow, while parameter C_{s1} is more informative than C_{s2}. The velocities of longitudinal waves C_p are the least informative for assessing the damage to rocks during bending.

The correlation R and determination R^2 coefficients and root mean square error (RMSE) are used to estimate the regression dependencies. The RMSE is a quantitative estimate of the absolute accuracy of the regression dependencies, by which one or several informative parameters allow others to be calculated. In this case, various combinations of acoustic parameters using regression dependencies allow us to estimate the damage of samples of gypsum-bearing rocks with different accuracies, estimated using RMSE. The smaller it is, the more accurate the dependence.

Let us estimate the error of the regression dependencies of various combinations of the informative parameters shown in Table 2 and Fig. 7–9. Calculations were made using the statistical software Statistica. Equations of linear multiple correlation were used for this. The results of the calculation of the correlation coefficient R, the coefficient of determination R^2, RMSE, as well as the ratios of these values for the appropriate combination of acoustic parameters and the velocity of longitudinal waves $RMSE_i/RMSE_{Cp}$, are presented in Table 3. The values of the regression dependence coefficients are not included in the table in order not to overload the text of the article.

Following from the data in Table 3, the dependence has the greatest error. The relative error values of other combinations of informative parameters are given in the last column on the right. They are all less than one. An increase in the number of informative parameters as a whole leads to a decrease in the RMSE. The best result is shown by the combination of all five informative parameters. The best dependence is:

$$\omega = -4{,}75611 + 0{,}00081 \cdot V_p - 0{,}00052 \cdot C_{s1} + \\ + 0{,}00074 \cdot C_{s2} + 0{,}01072 \cdot Q - 1{,}77719 \cdot Q_d \quad (4)$$

where R = 0,979, R^2 = 0,958 and RMSE = = 0,0239. The relative error of the prediction for damage ω = 0,356 after a series of cycles preceding the destruction is δ_ω = = 0,0239/0,356 = 0,067, i.e. less than 7%. The regression dependencies widely used in practice are based on the velocity of longitudinal waves. Their errors are much higher.

Table 3

Absolute and relative RMSE
Абсолютная и относительная RMSE

#	Informative Parameters	*R*	R^2	RMSE	$RMSE_i/RMSE_{Cp}$
1	C_p	0,287	0,083	0,1116	1,000
2	C_{s1}	0,799	0,639	0,0700	0,627
3	C_{s2}	0,369	0,136	0,1083	0,970
4	Q	0,296	0,088	0,1113	0,997
5	Qd	0,661	0,437	0,0874	0,783
6	C_p, C_{s1}	0,838	0,702	0,0637	0,570
7	C_p, C_{s2}	0,684	0,468	0,0850	0,762
8	C_p, Q	0,394	0,155	0,1071	0,960
9	C_{s1}, Q	0,884	0,782	0,0544	0,488
10	C_{s2}, Q	0,374	0,140	0,1081	0,968
11	C_p, Q_d	0,682	0,465	0,0853	0,764
12	C_{s1}, Q_d	0,963	0,927	0,0314	0,281
13	C_{s2}, Q_d	0,817	0,668	0,0672	0,602
14	Q, Q_d	0,936	0,877	0,0409	0,366
15	C_p, C_{s1}, C_{s2}	0,896	0,802	0,0518	0,464
16	C_p, C_{s1}, Q	0,929	0,863	0,0432	0,387
17	C_p, C_{s1}, Q_d	0,975	0,951	0,0257	0,230
18	C_p, C_{s2}, Q	0,897	0,804	0,0516	0,463
19	C_p, C_{s2}, Q_d	0,937	0,878	0,0407	0,365
20	C_p, C_{s1}, C_{s2}, Q	0,931	0,867	0,0425	0,381
21	C_p, C_{s1}, C_{s2}, Q_d	0,975	0,952	0,0256	0,230
22	C_p, C_{s1}, Q, Q_d	0,976	0,953	0,0254	0,227
23	C_p, C_{s2}, Q, Q_d	0,953	0,908	0,0355	0,317
24	C_p, C_{s1}, C_{s2}, Q, Q_d	0,979	0,958	0,0239	0,214

Conclusions

1. The change in the elastic wave velocities C_p, C_{s1}, C_{s2} and the acoustic quality factor Q of rock beams under cyclic bending loading are considered in the article. The specimen contained bonded dolomite-gypsum boundaries of complex structure. The number of loading cycles and damage parameter ω were registered. The elastic wave velocities decreased and the acoustic quality factor increased with an increase in the number of fatigue cycles. Just before destruction, the Q factor showed a sharp decrease associated with the destruction of the matrix. Finite element modelling confirmed the hypothesis that an increase in the quality factor is associated with a weakening of the contact strength at the boundaries between high-quality dolomite and low-quality gypsum.

2. Bending tests of the beam samples provided a figure for the loading of the sample in the stress state that is representative of the real one for the roof rocks of un-

derground mine workings. To reduce the testing time, the experiments were carried out in the mode of low cycle fatigue with predominantly plastic deformation. The samples were tested in a series of loads of 100 cycles, with an increase in the maximum load in each subsequent cycle. The regime of low cycle fatigue manifested itself in an abrupt change in the readings of the strain guage placed in the centre of the lower face of the sample, as well as in the increase of the AE event count rate $\dot{N}_e$ before destruction.

3. AE parameters were recorded. The damage parameter was estimated as $\omega_i = \Sigma N_{ei} / N_f$, where ω_i was the current value of the damage parameter after each *i*-th series of loads, ΣN_{ei} was the current value of the total AE event count from the beginning of the experiment and N_f was the total AE event count at destruction, $N_f = 5226$ imp. This made it possible to associate the damage parameter ω with the corresponding acoustic properties, which were measured before and between loading cycles.

4. The coefficients of the linear regression equations are obtained, which allow for the prediction of the damage parameter ω, depending on various combinations of acoustic properties, such as the velocity of the longitudinal and two transverse elastic waves, the acoustic quality factor and its derivative on the number of loading cycles. The accuracy of the obtained regression dependencies is estimated. The minimum error is achieved when using all informative acoustic parameters.

The authors are very grateful to the management and employees of Knauf Gips Novomoskovsk LLC, who provided the authors with samples of rock for testing. We also express our gratitude to V. Ivanov, P. Dubinin, A. Tyutcheva, A. Luchnikova and R. Nasibullin for their help in designing the laboratory setup and conducting experiments.

Авторы выражают благодарность руководству и сотрудникам ООО «Кнауф Гипс Новомосковск», предоставившим авторам образцы горных пород для испытаний. Мы также выражаем благодарность В.Б. Иванову, П.И. Дубинину, А.О. Лучниковой и Р.Р. Насибуллину за помощь в разработке лабораторной установки и проведении экспериментов.

СПИСОК ЛИТЕРАТУРЫ

1. *Li W., Bai J., Cheng J., Peng S., Liu H.* Determination of coal–rock interface strength by laboratory direct shear tests under constant normal load // International Journal of Rock Mechanics and Mining Science. 2015. Vol. 77. Pp. 60 – 67. DOI: 10.1016/j.ijrmms.2015.03.033.

2. *Krautblatter M., Funk D., Günzel F. K.* Why permafrost rocks become unstable. A rock-ice-mechanical model in time and space // Earth Surface Processes and Landforms. 2013. Vol. 38. Pp. 876 – 887. DOI: 10.1002/esp.3374.

3. *Бейсембаев К. М., Малыбаев Н. С., Тутанов С. К., Шманов М. Н.* Разработка модели лавы для системы управления механизированной крепью с обратной связью // Горный журнал. — 2019. — № 8. — С. 38 – 43. DOI. 10.17580/gzh.2019.08.07.

4. *Stanchits S., Burghardt J., Surdi A.* Hydraulic Fracturing of Heterogeneous Rock Monitored by Acoustic Emission // Rock Mechanics and Rock Engineering. 2015. Vol. 48. Pp. 2513 – 2527. DOI: 10.1007/s00603-015-0848-1.

5. *Zhong H., Ooi E. T., Song C., Ding T., Lin G., Li H.* Experimental and numerical study of the dependency of interface fracture in concrete-rock specimens on mode mixity // Engineering and Fracture Mechanics. 2014. Vol. 124 – 125. Pp. 287 – 309. DOI: 10.1016/j.engfracmech.2014.04.030.

6. *Carrubba P.* Skin friction on large-diameter piles socketed into rock // Canadian Geotechnical Journal. 1997. Vol. 34. Pp. 230 – 240. DOI: 10.1139/t96-104.

7. *Li Y., Liu W., Yang C., Daemen J. J. K.* Experimental investigation of mechanical behavior of bedded rock salt containing inclined interlayer // International Journal of Rock Mechanics and Mining Science. 2014. Vol. 69. Pp. 39 — 49. DOI: 10.1016/j.ijrmms.2014.03.006.

8. *Mets Y. S.* Study of blasting fatigue in rocks // Soviet Mining Science, 1983. Vol. 19. Pp. 37 — 42. DOI: 10.1007/BF02497962.

9. *Мец Ю. С.* Исследование влияния взрывных нагрузок различной интенсивности на сопротивляемость механическому разрушению крепких магнетитовых кварцитов // Физико-технические проблемы разработки полезных ископаемых. — 1982. — № 3. — С. 58 — 61.

10. *Labaune P., Rouabhi A.* Dilatancy and tensile criteria for salt cavern design in the context of cyclic loading for energy storage // Journal of Natural Gas Science and Engineering. 2019. Vol. 62. Pp. 314 — 329. DOI: 10.1016/j.jngse.2018.10.010.

11. *Kun G., Hailong L., Zhixin Y.* In-situ heavy and extra-heavy oil recovery. A review // Fuel. 2016. Vol. 185. Pp. 886 — 902. DOI: 10.1016/j.fuel.2016.08.047.

12. *Зайнагабдинов Д. А.*, *Быкова Н. М.* Транспортные тоннели и геодинамика горных массивов // Науковедение. Интернет-журнал. — 2014. — № 5 (24). Доступ: http://naukovedenie.ru/PDF/13KO514.pdf.

13. *Yang D., Zhang D., Niu S., Dang Y., Feng W., Ge S.* Experiment and study on mechanical property of sandstone post-peak under the cyclic loading and unloading // Geotechnical and Geological Engineering. 2018. Vol. 36. Pp. 1609 – 1620. DOI: 10.1007/s10706-017-0414-6.

14. *Cao A., Jing G., Ding Y., Liu S.* Mining-induced static and dynamic loading rate effect on rock damage and acoustic emission characteristic under uniaxial compression // Safety Science. 2019. Vol. 116. Pp. 86 — 96. Available at: https://linkinghub.elsevier.com/retrieve/pii/S0925753518318356.

15. *Винников В. А.*, *Захаров В. Н.*, *Малинникова О. Н.*, *Черепецкая Е. Б.* Исследование структуры и упругих свойств геоматериалов с помощью контактной широкополосной ультразвуковой структуроскопии // Горный журнал. — 2017. — № 4. — С. 24 — 32.

16. *Stoeckhert F., Molenda M., Brenne S., Alber M.* Fracture propagation in sandstone and slate — Laboratory experiments, acoustic emissions and fracture mechanics // Journal of Rock Mechanics and Geotechnical Engineering. 2015. Vol. 7. No 3. Pp. 237 — 249. Available at: https://linkinghub.elsevier.com/retrieve/pii/S1674775515000475.

17. *Работнов Ю. Н.* Введение в механику разрушения. — М.: Наука, 1987. — 80 с.

18. *Качанов Л. М.* Основы механики разрушения. — М.: Наука, 1974. — 312 с.

19. *Николенко П. В.*, *Шкуратник В. Л.*, *Чепур М. Д.* Акустико-эмиссионные эффекты при растяжении композитов и их использование для контроля состояния кровли горных выработок // Горный журнал. — 2019. — № 1. — С. 13 — 16. DOI: 10.17580/gzh.2019.01.03.

20. *Damaskinskaya E. E.*, *Panteleev I. A.*, *Gafurova D. R.*, *Frolov D. I.* Structure of a deformed inhomogeneous material on the data of acoustic emission and X-Ray computer microtomography // Physics of the Solid State. 2018. Vol. 60. No 7. Pp. 1363 — 1367. DOI: 10.1134/S1063783418070077.

21. *Тихоцкий С. А., Фокин И. В., Баюк И. О., Белобородов Д. Е. и др.* Комплексные лабораторные исследования керна в ЦПГИ ИФЗ РАН // Наука и технологические разработки. — 2017. — Т. 96. — № 2. — С. 17 — 32. DOI: 10.21455/std2017.2-2.

22. *Lebedev A. V.*, *Ostrovskii L. A.*, *Sutin A. M.*, *Soustova I. A.*, *Johnson P. A.* Resonant acoustic spectroscopy at low Q factors // Acoustical Physics. 2003. Vol. 49. No 1. Pp. 81 — 87. DOI: 10.1134/1.1537392.

23. *Вознесенский А. С., Красилов М. Н., Куткин Я. О., Тавостин М. Н.* Лабораторная система для расширенных испытаний образцов горных пород при изгибе // Горный информационно-аналитический бюллетень. — 2018. — № 10. — С. 132–137. DOI: 10.25018/0236-1493-2018-10-0-132-137.

24. *Пономарев С. В.*, *Рикконен С. В.*, *Азин А. В.*, *Каравацкий А. К.*, *Марицкий Н. Н.*, *Пономарев С. А.* Применение метода акустической эмиссии для моделирования долговечности металлических элементов строительных конструкций / Перспективные материалы

в строительстве и технике (ПМСТ-2014). Материалы Международной научной конференции молодых ученых. — Томск, 2014. — С. 557 — 565. ГИАБ

REFERENCES

1. Li W., Bai J., Cheng J., Peng S., Liu H. Determination of coal–rock interface strength by laboratory direct shear tests under constant normal load. *International Journal of Rock Mechanics and Mining Science*. 2015. Vol. 77. Pp. 60 — 67. DOI: 10.1016/j.ijrmms.2015.03.033.

2. Krautblatter M., Funk D., Günzel F. K. Why permafrost rocks become unstable. A rock-ice-mechanical model in time and space. *Earth Surface Processes and Landforms*. 2013. Vol. 38. Pp. 876 — 887. DOI: 10.1002/esp.3374.

3. Beysembaev K. M., Malybaev N. S., Tutanov S. K., Shmanov M. N. Longwall model for feedback control of powered roof support. *Gornyi Zhurnal*. 2019, no 8, pp. 38 — 43. [In Russ]. DOI. 10.17580/gzh.2019.08.07.

4. Stanchits S., Burghardt J., Surdi A. Hydraulic Fracturing of Heterogeneous Rock Monitored by Acoustic Emission. *Rock Mechanics and Rock Engineering*. 2015. Vol. 48. Pp. 2513 — 2527. DOI: 10.1007/s00603-015-0848-1.

5. Zhong H., Ooi E. T., Song C., Ding T., Lin G., Li H. Experimental and numerical study of the dependency of interface fracture in concrete-rock specimens on mode mixity. *Engineering and Fracture Mechanics*. 2014. Vol. 124 — 125. Pp. 287 — 309. DOI: 10.1016/j.engfracmech.2014.04.030.

6. Carrubba P. Skin friction on large-diameter piles socketed into rock. *Canadian Geotechnical Journal*. 1997. Vol. 34. Pp. 230 — 240. DOI: 10.1139/t96-104.

7. Li Y., Liu W., Yang C., Daemen J. J. K. Experimental investigation of mechanical behavior of bedded rock salt containing inclined interlayer. *International Journal of Rock Mechanics and Mining Science*. 2014. Vol. 69. Pp. 39 — 49. DOI: 10.1016/j.ijrmms.2014.03.006.

8. Mets Y. S. Study of blasting fatigue in rocks. *Soviet Mining Science*, 1983. Vol. 19. Pp. 37 — 42. DOI: 10.1007/BF02497962.

9. Mets Yu. S. Effect of blast load of varying intensity upon the resistance to mechanical destruction in strong magnetite quartzites. *Fiziko-tekhnicheskiye problemy razrabotki poleznykh iskopayemykh*. 1982, no 3, pp. 58 — 61. [In Russ].

10. Labaune P., Rouabhi A. Dilatancy and tensile criteria for salt cavern design in the context of cyclic loading for energy storage. *Journal of Natural Gas Science and Engineering*. 2019. Vol. 62. Pp. 314 — 329. DOI: 10.1016/j.jngse.2018.10.010.

11. Kun G., Hailong L., Zhixin Y. In-situ heavy and extra-heavy oil recovery. A review. *Fuel*. 2016. Vol. 185. Pp. 886 — 902. DOI: 10.1016/j.fuel.2016.08.047.

12. Zaynagabdinov D.A., Bykova N. M. Transport tunnels and geodynamics of mountain ranges. *Naukovedenie. Internet-zhurnal.* 2014, no 5 (24). [In Russ]. Available at: http://naukovedenie.ru/PDF/13KO514.pdf.

13. Yang D., Zhang D., Niu S., Dang Y., Feng W., Ge S. Experiment and study on mechanical property of sandstone post-peak under the cyclic loading and unloading. *Geotechnical and Geological Engineering*. 2018. Vol. 36. Pp. 1609 – 1620. DOI: 10.1007/s10706-017-0414-6.

14. Cao A., Jing G., Ding Y., Liu S. Mining-induced static and dynamic loading rate effect on rock damage and acoustic emission characteristic under uniaxial compression. *Safety Science*. 2019. Vol. 116. Pp. 86 — 96. Available at: https://linkinghub.elsevier.com/retrieve/pii/S0925753518318356.

15. Vinnikov V.A., Zakharov V. N., Malinnikova O. N., Cherepetskaya E. B. Analysis of structure and elastic properties of geomaterials using contact broadband ultrasonic structural spectroscopy. *Gornyi Zhurnal*. 2017, no 4, pp. 24 — 32. [In Russ].

16. Stoeckhert F., Molenda M., Brenne S., Alber M. Fracture propagation in sandstone and slate — Laboratory experiments, acoustic emissions and fracture mechanics. *Journal of Rock Mechanics and Geotechnical Engineering*. 2015. Vol. 7. No 3. Pp. 237 — 249. Available at: https://linkinghub.elsevier.com/retrieve/pii/S1674775515000475.

17. Rabotnov Yu. N. *Vvedenie v mekhaniku razrusheniya* [Introduction to fracture mechanics], Moscow, Nauka, 1987, 80 p.

18. Kachanov L. M. *Osnovy mekhaniki razrusheniya* [Fundamentals of fracture mechanics], Moscow, Nauka, 1974, 312 p.

19. Nikolenko P. V., Shkuratnik V. L., Chepur M. D. Acoustic emission effects in tension of composites and practical applications for roof control in underground mines. *Gornyi Zhurnal*. 2019, no 1, pp. 13—16. [In Russ]. DOI: 10.17580/gzh.2019.01.03.

20. Damaskinskaya E. E., Panteleev I. A., Gafurova D. R., Frolov D. I. Structure of a deformed inhomogeneous material on the data of acoustic emission and X-Ray computer microtomography. *Physics of the Solid State*. 2018. Vol. 60. No 7. Pp. 1363—1367. DOI: 10.1134/S1063783418070077.

21. Tikhotskiy S. A., Fokin I. V., Bayuk I. O., Beloborodov D. E. Comprehensive core laboratory tests at TsPGI IPE RAS. *Nauka i tekhnologicheskie razrabotki*. 2017. vol. 96, no 2. C. 17—32. [In Russ]. DOI: 10.21455/std2017.2-2.

22. Lebedev A. V., Ostrovskii L. A., Sutin A. M., Soustova I. A., Johnson P. A. Resonant acoustic spectroscopy at low Q factors. *Acoustical Physics*. 2003. Vol. 49. No 1. Pp. 81—87. DOI: 10.1134/1.1537392.

23. Voznesenskiy A.S., Krasilov M.N., Kutkin Ya.O., Tavostin M.N. Laboratory system for expanded bending tests of rock specimens. *MIAB. Mining Inf. Anal. Bull.* 2018, no 10, pp. 132–137. [In Russ]. DOI: 10.25018/0236-1493-2018-10-0-132-137.

24. Ponomarev S. V., Rikkonen S. V., Azin A. V., Karavatskiy A. K., Maritskiy N. N., Ponomarev S. A. The use of acoustic emission method for modeling the durability of the metal elements of building structures. *Perspektivnye materialy v stroitel'stve i tekhnike (PMST-2014)*. Materialy Mezhdunarodnoy nauchnoy konferentsii molodykh uchenykh [Advanced materials in construction and engineering (PMST-2014) Materials of the International Scientific Conference of Young Scientists], Tomsk, 2014, pp. 557—565. [In Russ].

ИНФОРМАЦИЯ ОБ АВТОРАХ

Вознесенский Александр Сергеевич[1] — д-р техн. наук, профессор, e-mail: al48@mail.ru,
Красилов Максим Николаевич[1] — аспирант, e-mail: krasilov.maksim.93@mail.ru,
Куткин Ярослав Олегович[1] — канд. техн. наук, доцент, e-mail: kutnew@mail.ru,
Тютчева Анастасия Олеговна[1] — аспирант, e-mail: 9295947810@mail.ru,
[1] ГИ НИТУ «МИСиС».
Для контактов: Вознесенский А.С., e-mail: al48@mail.ru.

INFORMATION ABOUT THE AUTHORS

A.S. Voznesenskii[1], Dr. Sci. (Eng.), Professor, e-mail: al48@mail.ru,
M.N. Krasilov[1], Graduate Student, e-mail: krasilov.maksim.93@mail.ru,
Ya.O. Kutkin[1], Cand. Sci. (Eng.), Assistant Professor, e-mail: kutnew@mail.ru,
A.O. Tyutcheva[1], Graduate Student, e-mail: 9295947810@mail.ru,
[1] Mining Institute, National University of Science and Technology «MISiS», 119049, Moscow, Russia.
Corresponding author: A.S. Voznesenskii, e-mail: al48@mail.ru.

Получена редакцией 17.03.2020; получена после рецензии 21.04.2020; принята к печати 20.06.2020.
Received by the editors 17.03.2020; received after the review 21.04.2020; accepted for printing 20.06.2020.

ОБОСНОВАНИЕ И РАЗРАБОТКА СХЕМЫ ПЕРЕДВИЖКИ СЕКЦИЙ МЕХАНИЗИРОВАННОЙ КРЕПИ В УСЛОВИЯХ ОТРАБОТКИ ПЛАСТОВ С НЕУСТОЙЧИВЫМИ КРОВЛЯМИ

(2020, № 1, СВ 3, 12 с.)

Турбор Ирина Александровна[1] — соискатель,
Турук Юрий Владимирович[1] — д-р техн. наук, профессор, e-mail: uraturuk@mail.ru,
Шурыгин Дмитрий Николаевич[1] — д-р техн. наук, доцент,
[1] Южно-Российский государственный политехнический университет (НПИ) имени М.И. Платова.

Основной функцией механизированной крепи является поддержание и сохранение целостности непосредственной кровли пласта, то есть предотвращение расслоения и образования вывалов породы в призабойном пространстве, а также в обеспечении требуемой скорости крепления в экстремальных ситуациях. Данная функция решается путем выбора эффективных схем расстановки и передвижки секций механизированной крепи. Проанализированы существующие схемы передвижки секций механизированной крепи и результаты работы механизированных комплексов с различными схемами передвижки, установлены их особенности и недостатки, которые не позволяют обеспечить оптимальные параметры работы лав в условиях с неустойчивыми кровлями. Обоснована необходимость разработки комбинированной схемы передвижки секций механизированной крепи. Особенностью комбинированной схемы, в отличии от существующих, является опережающая передвижка секций механизированной крепи за проходом исполнительного органа комбайна и последующая задвижка не передвинутых. Установлено, что численность обслуживающего персонала для передвижки секций при комбинированной схеме следует определять из отношения скорости движения комбайна и скорости крепления. Применение комбинированной схемы в условиях Обособленного предприятия «Шахтоуправление «Трудовское» позволило увеличить скорость крепления в очистном забое до трех раз. При этом были сняты ограничения на скорость выемки по фактору крепления и повышена устойчивость непосредственной кровли пласта. Возникающие при задержке передвижки секций обнажения находились в допустимых пределах для неустойчивых кровель. Применение комбинированной схемы передвижки секций механизированной крепи позволило снизить конвергенцию вмещающих пород на 25–30% и вывалообразования в призабойном пространстве. Таким образом, комбинированная схема передвижки секций крепи является более безопасной и эффективной.

Ключевые слова: механизированная крепь, секция крепи, очистной забой, схема передвижки, неустойчивая кровля, скорость крепления, призабойное пространство, вывалообразование.

JUSTIFICATION AND DEVELOPMENT OF A SCHEME FOR MOVING SECTIONS OF MECHANIZED SUPPORT IN THE CONDITIONS OF MINING LAYERS WITH UNSTABLE ROOFS

I.A. Turbor[1], Applicant, *Yu.V. Turuk*[1], Dr. Sci. (Eng.), Professor, e-mail: uraturuk@mail.ru,
D.N. Shurygin[1], Dr. Sci. (Eng.), Assistant Professor,
[1] Platov South-Russian State Polytechnic University (NPI), 346428, Novocherkassk, Russia.

Analyzed the existing scheme of shifting sections of powered roof support and the work of mechanized complexes with different schemes of advancing, set their features and flaws that do not allow for the optimal parameters of longwalls in areas that have fragile roofs. The necessity of developing a combined scheme for moving sections of mechanized support is justified. A special feature of the combined scheme, in contrast to the existing ones, is the advance movement of sections of mechanized support behind the passage of the executive body of the combine and the subsequent valve of the non-moved ones. It is established that the number of service personnel for moving sections in the combined scheme should be determined from the ratio of the speed of movement of the combine and the speed of attachment. The use of the combined scheme in the conditions of the Separate enterprise «Trudovskoye mine management» allowed to increase the speed of fastening in the treatment face up to three times. At the same time, restrictions on the speed of excavation by the attachment factor were removed and the stability of the immediate roof of the formation was increased. Arising from the delay in the relocation of sections of the outcrops were in the acceptable range for unstable roofs. The use of a combined scheme for moving sections of mechanized support allowed to reduce the convergence of host rocks by 25—30% and fallout in the bottom-hole space. Thus, the combined scheme of moving the support sections is safer and more efficient.

Key words: mechanized lining, lining section, working face, movement pattern, unstable roof, fastening speed, bottom-hole space, dumping.